



Cite this: *Chem. Commun.*, 2020, **56**, 6583

Received 8th April 2020,  
Accepted 5th May 2020

DOI: 10.1039/d0cc02525a

[rsc.li/chemcomm](http://rsc.li/chemcomm)

## All-metal $\sigma$ -antiaromaticity in dimeric cluster anion $\{[\text{CuGe}_9\text{Mes}]_2\}^{4-}\dagger$

Zi-Chuan Wang, <sup>a</sup> Nikolay V. Tkachenko, <sup>b</sup> Lei Qiao, <sup>a</sup> Eduard Matito, <sup>cd</sup> Alvaro Muñoz-Castro, <sup>e</sup> Alexander I. Boldyrev <sup>\*b</sup> and Zhong-Ming Sun <sup>\*a</sup>

**In this work, we report a dimeric cluster anion,  $\{[\text{CuGe}_9\text{Mes}]_2\}^{4-}$ , which was isolated as the  $[\text{K}(2,2,2\text{-crypt})]^+$  salt and characterized by using single-crystal X-ray diffraction and ESI mass spectroscopy. The title cluster represents the first locally  $\sigma$ -antiaromatic compound in the solid state, as well as the first heteroatomic antiaromatic compound.**

Aromaticity and antiaromaticity are two of the most extensively studied concepts in chemistry,<sup>1</sup> which can be demonstrated by the over 189 800 articles involving aromaticity or antiaromaticity published in the last 10 years.<sup>2</sup> The concept of anti-aromaticity was proposed by Breslow in his pioneering paper in 1965, intending to describe the destabilization of compounds caused by the 4n  $\pi$ -electron system.<sup>3</sup> In 2003, Wang *et al.* observed all-metal anti-aromatic  $\text{Al}_4^{4-}$  rectangles in  $\text{Li}_3\text{Al}_4^{4-}$  anions by using photoelectron spectroscopy.<sup>4</sup> This was the first time that the concept of anti-aromaticity was expanded from organic compounds to metal clusters. Subsequently, a series of antiaromatic metal clusters has been studied in the gas phase, such as  $\pi$ -antiaromatic  $[\text{Al}_3\text{H}_3]^{2-}$ ,<sup>5</sup> and  $\sigma$ -antiaromatic anionic  $\text{Li}_3^-$  and neutral  $\text{Li}_4$ .<sup>6</sup> Besides the homoatomic cases mentioned above, heteroatomic antiaromatic fragments were also investigated by both experimental and theoretical chemists. 1,3,2,4-Diazadiboretiidine ( $\text{B}_2\text{N}_2\text{H}_4$ ) was once considered to be antiaromatic because it is an isoelectronic system to cyclobutadiene ( $\text{C}_4\text{H}_4$ ), which is a recognized antiaromatic model compound. However, due to the electronegativity difference between boron and nitrogen atoms,

the electrons could not be effectively delocalized.<sup>7</sup> Thus, the actual synthesized  $\text{B}_2\text{N}_2\text{H}_4$  derivatives did not exhibit antiaromatic properties as predicted before.<sup>8</sup> Although the research on antiaromaticity of metal clusters has made great progress in theoretical chemistry, the corresponding products in the solid phase have hardly been verified so far, especially compared to the aromatic species.<sup>9</sup> Our group has been working on the synthesis of aromatic clusters.<sup>10</sup> In 2016, our group synthesized the first all-metal  $\pi$ -antiaromatic complex,  $[\text{Ln}(\eta^4\text{-Sb}_4)_3]^{3-}$  ( $\text{Ln} = \text{La, Ho, Y, Er, Lu}$ ), in the solid state. The strong interaction between the lanthanide cation and three *cyclo*- $\text{Sb}_4$  plays an important role in the stabilization of the highly reactive antiaromatic  $\text{Sb}_4$  units.<sup>10c</sup> In the current work, we report the first case of all-metal  $\sigma$ -antiaromaticity in a synthesized anionic metal cluster,  $\{[\text{CuGe}_9\text{Mes}]_2\}^{4-}$ , in which the heteroatomic antiaromatic  $\text{Cu}_2\text{Ge}_2$  unit is stabilized by multiple local  $\sigma$ -aromatic germanium clusters.

The compound  $\{[\text{CuGe}_9\text{Mes}]_2\}^{4-}$  (**1**) crystallized in the form of  $[\text{K}(2,2,2\text{-crypt})]_4\cdot\text{1}\cdot(\text{DMF})_3$  was isolated in a DMF solution of Zintl phase  $\text{K}_4\text{Ge}_9$ , mesityl-copper ( $\text{CuMes}$ ), and 2,2,2-crypt(4,7,13,16,21,24-hexaoxa-1,10-diazabicyclo [8.8.8] hexacosane), possessing triclinic space group  $\bar{P}\bar{1}$  symmetry. As exhibited in Fig. 1, the anion species can be viewed as a dimer of  $[\text{CuGe}_9(\text{Mes})]^{2-}$ , where a Cu atom and a substituted Ge were located at the apexes of the bicapped square antiprism of  $\text{CuGe}_9$ , respectively. A capped copper atom and a germanium atom at the waist of the cage from each subunit formed a diamond structure that

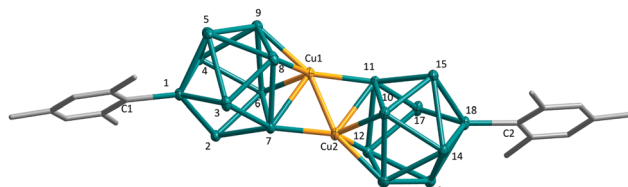


**Fig. 1** Structure of  $\{[\text{CuGe}_9\text{Mes}]_2\}^{4-}$ ; thermal ellipsoids are drawn at the 50% probability level. Selected interatomic distances [ $\text{\AA}$ ]: Cu1–Cu2 2.5214(7), Cu1–Ge7 2.6072(6), Cu2–Ge7 2.4007(6), Cu1–Ge11 2.4301(6), Cu2–Ge11 2.5998(6), C1–Ge1 1.998(3), Ge2–Ge3 3.4817(6), Ge2–Ge4 2.9514(6).

<sup>a</sup> School of Materials Science and Engineering, State Key Laboratory of Element-Organic Chemistry, Tianjin Key Lab for Rare Earth Materials and Applications, Nankai University, Tianjin 300350, China. E-mail: sunlab@nankai.edu.cn

<sup>b</sup> Department of Chemistry and Biochemistry, Utah State University 0300 Old Main Hill, Logan, UT 84322-0300, USA. E-mail: a.i.boldyrev@usu.edu

<sup>c</sup> Donostia International Physics Center (DIPC), Donostia 20080, Euskadi, Spain

<sup>d</sup> IKERBASQUE, Basque Foundation for Science, Bilbao 48011, Euskadi, Spain

<sup>e</sup> Grupo de Química Inorgánica y Materiales Moleculares, Facultad de Ingeniería, Universidad Autónoma de Chile, El Llano Subercaseaux, Santiago 2801, Chile

<sup>†</sup> Electronic supplementary information (ESI) available. CCDC 1974758. For ESI and crystallographic data in CIF or other electronic format see DOI: 10.1039/d0cc02525a

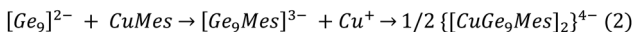
<sup>‡</sup> These authors contributed equally.

connected the two subunits.  $[\text{Cu}_2\text{Ge}_{18}(\text{Mes})_2]^{4-}$  presented a pseudo- $C_{2h}$  symmetric structure with  $\text{Cu}_2\text{Ge}_2$  diamond as the symmetry plane. Compared to other similar 10-atomic *closo*-cluster cages such as  $[\text{Ge}_9\text{ZnPh}]^{3-}$ <sup>11a</sup>  $[\text{Ge}_9\text{CuP}^{\text{I}}\text{Pr}_3]^{3-}$ <sup>11b</sup> or  $[\text{Ge}_9\text{Pd}(\text{PPh})_3]^{3-}$ <sup>11c</sup>  $[\text{Cu}_2\text{Ge}_{18}(\text{Mes})_2]^{4-}$  has an enlarged and slightly corrugated skeleton. The Ge-Ge bond lengths within the squares adjacent to the Cu atoms (Ge6-Ge9 and Ge10-Ge13) range from 2.6854(6) to 2.7730(6), which differ little in comparison to those of other similar species. However, the Ge-Ge contacts within the squares adjacent to Ge1 and Ge18 were elongated to the range of 2.8171(6)-3.337(0), which are much longer than any adjacent Ge-Ge distance in the reported Ge clusters or in the electron-deficient oxidation coupling Ge clusters, such as  $[\text{Ge}_9]^{2-}$ <sup>12a</sup>  $[\text{Ge}_9-\text{Ge}_9]^{6-}$ <sup>12b</sup>  $[\text{Ge}_9=\text{Ge}_9=\text{Ge}_9]^{6-}$ <sup>12c</sup> and  $[\text{Ge}_9=\text{Ge}_9=\text{Ge}_9=\text{Ge}_9]^{8-}$ <sup>12d</sup>. This was probably caused by the electron-withdrawing effect of the mesityl group together with the formation of  $\text{Cu}_2\text{Ge}_2$  diamond.

The average Cu-Ge bond length in **1** was 2.500(6), which was similar to that in functionalized germanium clusters such as  $\text{R}_6\text{Ge}_{18}\text{Cu}$  ( $\text{R} = \text{Si}(\text{SiMe}_3)_3$ ) (2.622 Å)<sup>13a</sup> and  $(\text{Ge}_9\text{R}_3)\text{Cu}(\text{Ge}_9\text{R}_3)\text{CuPPPh}_3$  (2.571 Å),<sup>13b</sup> while it was longer than the Ge-Cu σ-bond distance (2.362(1)) in  $[\text{Cu}(\eta^4\text{-Ge}_9)(\eta^1\text{-Ge}_9)]^{7-}$ .<sup>11b</sup> Interestingly, in  $\text{Cu}_2\text{Ge}_2$  diamond, the average length of Cu1-Ge7 and Cu2-Ge11(2.6035(6)) are obviously longer than that of Cu2-Ge7 and Cu1-Ge11 (2.4154(6)), indicating that Cu seems to have a stronger interaction with its opposite cluster than with its own subunit. This phenomenon is also found in  $\{[\text{CuSn}_5\text{Sb}_3]^{2-}\}_2$ , where Cu atoms are also closer to the opposite cages.<sup>14</sup>

The formation of compound **1** is likely to be derived from the oxidation of  $\text{K}_4\text{Ge}_9$  with 2 equiv. of excess CuMes in the first step of the reaction, followed by nucleophilic substitution of Mes<sup>-</sup> to generate  $[\text{Ge}_9\text{Mes}]^{3-}$  species, which exhibited a strong signal ( $[\text{K}(2,2,2\text{-crypt})]\text{[Ge}_9\text{Mes}]^{3-}$ ,  $m/z = 1188.61$ ) in the ESI-MS spectrum (Fig. S4, ESI†). Subsequently,  $[\text{Ge}_9\text{Mes}]^{3-}$  assembled with a copper cation, leading to the formation of a dimeric cluster (Scheme 1). The signals of the byproducts  $\text{Ge}_9\text{Mes}_2$  and  $\text{Ge}_{18}\text{Mes}_2$  were also detected, suggesting that the  $[\text{Ge}_9\text{Mes}]^{3-}$  species is relatively stable and its evolution to **1** is not a unique approach. Nevertheless, the formed compound **1** kept a complete structure that showed a strong signal in the mass spectrum (Fig. 2). In our pretest study, reaction of  $\text{K}_4\text{Ge}_9$  with 1 or 2 equiv. of CuMes in ethylenediamine only yielded a copper mirror and an amorphous germanium precipitate, suggesting that  $\text{Cu}^+$  can effectively oxidize the  $\text{Ge}_9$  cluster but cannot assemble into endohedral intermetallic clusters like  $[\text{Cu}@\text{Sn}_5]^{3-}$  and  $[\text{Cu}@\text{Pb}_9]^{3-}$ .<sup>15</sup>

Compared with  $\eta^4:\eta^1$  coordinated  $[\text{Cu}(\eta^4\text{-Ge}_9)(\eta^1\text{-Ge}_9)]^{7-}$ ,<sup>11b</sup>  $\eta^3:\eta^3$  coordinated  $(\text{Ge}_9\text{R}_3)\text{Cu}(\text{Ge}_9\text{R}_3)\text{CuPPPh}_3$ ,<sup>13b</sup> and face-fused  $[\text{Ge}_{18}\text{Pd}_3(\text{Sn}^{\text{I}}\text{Pr}_3)_6]^{2-}$ ,<sup>13c</sup> compound **1** has a novel linkage manner for dimeric Zintl germanium clusters. In order to understand the chemical bonding in the  $\{[\text{CuGe}_9\text{Mes}]_2\}^{4-}$  cluster, we first performed an Adaptive Natural Density Partitioning (AdNDP)<sup>6b,16</sup> analysis of the



Scheme 1 Possible mechanisms for the formation of **1**.

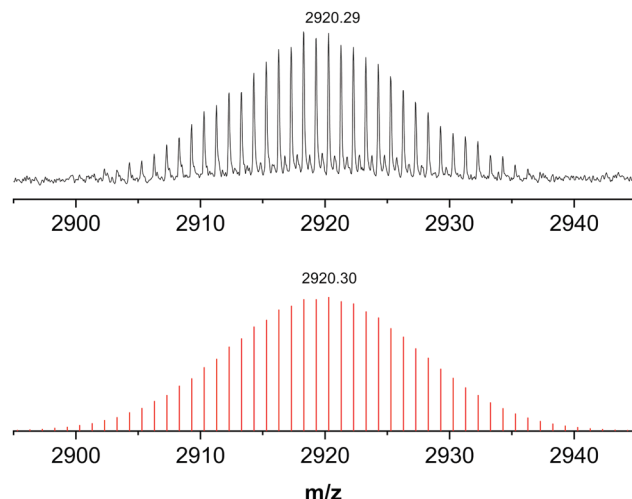


Fig. 2 Negative-ion ESI mass spectrum of **1**. Measured (top) and simulated (bottom) spectrum of the fragment  $[\text{K}(2,2,2\text{-crypt})]_3[\text{Cu}_2\text{Ge}_{18}\text{Mes}_2]^-$ .

monomeric  $[\text{CuGe}_9\text{Mes}]^{2-}$  (**2**) species. The optimized monomeric structure belongs to the  $C_s$  symmetry group while the metal cluster part is  $C_{4v}$ -symmetric and can be described as a twice capped square antiprism (Fig. 3). The 96 valence electrons of the whole structure were localized into 48 bonding elements, which could be divided into organic and metal cluster parts. The organic ligand consists of twenty 2-center 2-electron (2c-2e) C-C and C-H σ-bonds with occupation numbers (ONs) in the range of 1.99–1.97 |e|, and three 6c-2e π-aromatic bonds within the six-membered carbon ring (ON = 1.99–1.96 |e|). The Mes ligand is bound to the  $\text{Ge}_9\text{Cu}$  cage via the 2c-2e Ge-C σ-bond with ON = 1.96 |e| (Fig. 3b). The remaining 48 electrons are responsible for binding interactions inside the  $C_{4v}$ -symmetric metal cage. We found five classical Lewis d-type lone pairs on the Cu-atom (ON = 1.99–1.96 |e|),

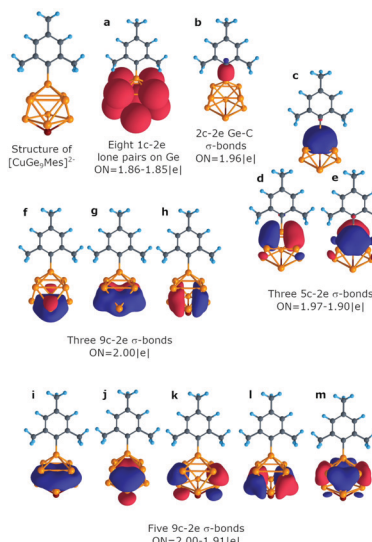


Fig. 3 Chemical bonding picture of the  $\text{CuGe}_9$  fragment obtained for the  $[\text{CuGe}_9\text{Mes}]^{2-}$  cluster. ON denotes the occupation number (2.00 |e| in an ideal case). Lines between atoms help in visualization and do not necessarily represent 2c-2e bonds here and elsewhere.

eight s-type lone pairs on Ge-atoms (Fig. 3a), and eleven multicenter delocalized  $\sigma$ -bonds with  $ON = 2.00\text{--}1.91|e|$  (Fig. 3c-m). The latter eleven bonds are responsible for the bonding inside the three areas in the  $\text{Ge}_9\text{Cu}$  cage. The first area, the  $\text{Ge}_5$  cap fragment, contains three 5c-2e  $\sigma$ -bonds with  $ON = 1.97\text{--}1.90|e|$  (Fig. 3c-e). Another area is the  $\text{CuGe}_4$  cap fragment with three 9c-2e  $\sigma$ -bonds (Fig. 3f-h). Although these bonds were found to be 9-center, we should indicate them as  $\text{CuGe}_4$  and not as  $\text{CuGe}_8$  bonds, because of the large contribution of the  $\text{CuGe}_4$  fragment ( $\sim 99\text{--}80\%$ ). The remaining five 9c-2e bonds (Fig. 3i-m) are responsible for binding of the  $\text{Ge}_8$  antiprism ( $\sim 99\text{--}97\%$  contribution from germanium atoms). All three described fragments satisfy the Hückel electron counting rule and could be described as  $\sigma$ -aromatic. The complete bonding pattern of  $[\text{CuGe}_9\text{Mes}]^{2-}$  can be found in the ESI† (Fig. S10). Notably, the local  $\sigma$ -aromatic description of  $[\text{CuGe}_9\text{Mes}]^{2-}$  agrees with the previously discussed bonding in the  $C_{4v}\text{-}[\text{Ge}_9]^{4-}$  cluster that possesses the same electron localization features and could be described with multiple local  $\sigma$ -aromatic fragments.<sup>17</sup>

Following the insights obtained on the monomeric species, we performed an AdNDP analysis of the novel dimeric  $C_{2h}$   $\{[\text{CuGe}_9\text{Mes}]_2\}^{4-}$  cluster (Fig. S11, ESI†). The optimized geometry is in good agreement with the experimental structure (Table S2, ESI†). We found that the bonding pattern of  $[\text{CuGe}_9\text{Mes}]^{2-}$  monomers in the dimeric cluster is almost preserved. Each monomer consists of a  $\pi$ -aromatic organic part bound to the metal cage *via* a Ge-C  $\sigma$ -bond, twenty-four lone pairs on Cu and Ge atoms, and three locally  $\sigma$ -aromatic fragments inside the  $\text{CuGe}_8$  cage. The main difference in bonding patterns of **1** and **2** lies in the number of germanium lone pairs. Only fourteen lone pairs were localized for **1**, while the remaining two germanium atoms in square antiprisms (Ge7 and Ge11) donate their four electrons (two electrons per each germanium) and form two 3c-2e  $\sigma$ -bonds ( $ON = 1.92|e|$ ) responsible for binding the two monomers (Fig. S18, ESI†). The contribution of Ge atoms to these bonds is found to be  $\sim 84\%$ . We note that these two bonds could also be found as 4c-2e with  $ON = 1.93\text{--}1.92|e|$ . Thus, the interaction within the  $\text{Cu}_2\text{Ge}_2$  diamond is the main difference between the bonding patterns of monomer **2** and dimer **1**. The shape of the fragment, the chemical bonding picture, and the number of electrons (4e) render this interaction as antiaromatic. For a previously investigated  $\text{Li}_4$   $\sigma$ -antiaromatic molecule, it was shown that the square geometry is unstable, and the global minimum structure is diamond shaped. Moreover, the antiaromaticity of  $\text{Li}_4$  leads to the formation of locally 3c-2e  $\sigma$ -aromatic islands within the two  $\text{Li}_3$  triangles.<sup>6b</sup> The same behavior is observed for the  $\text{Cu}_2\text{Ge}_2$  fragment. We want to note that the binding interactions between two monomers could also be described in terms of Wade–Mingos electron counting rules.<sup>18</sup> A detailed description can be found in the ESI.†

In order to further prove the antiaromaticity of the  $\text{Cu}_2\text{Ge}_2$  fragment, we chose the most typical  $\text{NICS}_{\text{iso}}$  and  $\text{NICS}_{\text{zz}}$  indices<sup>19</sup> to perform analysis at special points of compound **1**. The highly positive  $\text{NICS}_{\text{zz}}$  values agree with the antiaromatic description of the fragment. Moreover, the change of  $\text{NICS}_{\text{zz}}$  with the distance from the center of the  $\text{Cu}_2\text{Ge}_2$  fragment agrees nicely with the

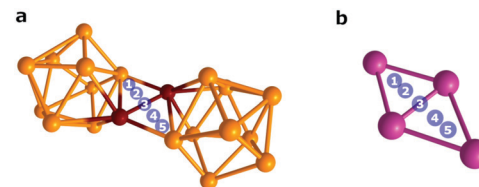


Fig. 4  $\{[\text{CuGe}_9\text{Mes}]_2\}^{4-}$  (a) and  $\text{Li}_4$  (b) clusters with points that were selected for calculation of NICS indices. Organic ligands are omitted for clarity.

Table 1  $\text{NICS}_{\text{iso}}$  and  $\text{NICS}_{\text{zz}}$  indices calculated for  $\{[\text{CuGe}_9\text{Mes}]_2\}^{4-}$  and  $\text{Li}_4$

Point	$\{[\text{CuGe}_9\text{Mes}]_2\}^{4-}$		$\text{Li}_4$	
	$\text{NICS}_{\text{iso}}$	$\text{NICS}_{\text{zz}}$	$\text{NICS}_{\text{iso}}$	$\text{NICS}_{\text{zz}}$
1	-44.59	2.11	-5.33	-1.18
2	-24.83	14.52	0.88	5.16
3	-19.45	18.09	6.41	9.01
4	-24.83	14.52	0.88	5.16
5	-44.59	2.11	-5.33	-1.18

same results obtained for the antiaromatic  $\text{Li}_4$  cluster (Fig. 4 and Table 1). The analysis of NICS for other points also confirmed the  $\sigma$ -antiaromatic nature of compound **1** (Fig. S12 and Table S4, ESI†).

In Fig. 5, the global magnetic behavior of the monomer and dimer is given in terms of an averaged specific orientation of the applied field, related to  $\text{NICS}_{\text{iso}}(\mathbf{B}_{\text{iso}}^{\text{ind}})$  and  $\text{NICS}_{\text{zz}}(\mathbf{B}_{\text{zz}}^{\text{ind}})$ . This supports the aromatic behavior of the  $\text{CuGe}_9$  cage, besides the mesityl group, in the monomer, as denoted by the shielding region from  $\mathbf{B}_{\text{iso}}^{\text{ind}}$ , and shielding cone behavior from the different orientation for the former cage. It is worth noting that the formation of the  $\{[\text{CuGe}_9\text{Mes}]_2\}^{4-}$  cluster introduces strong changes as a result of the antiaromatic character of the  $\text{Cu}_2\text{Ge}_2$  fragment given by its pair of locally 3c-2e  $\sigma$ -aromatic islands. This generates a deshielding region above the central  $\text{Cu}_2\text{Ge}_2$  diamond in the  $\mathbf{B}_{\text{iso}}^{\text{ind}}$  representation, which is enhanced under a parallel field ( $\mathbf{B}_z^{\text{ind}}$ ), as is distinctive for antiaromatic rings as accounted by  $\text{NICS}_{\text{zz}}$ . For  $x$ - and  $y$ -orientations, the aromatic character of the  $\text{CuGe}_9$  cage contributes to the shielding response at  $\text{Cu}_2\text{Ge}_2$ , leading to a negative  $\text{NICS}_{\text{iso}}$  index. The contour plot representation (Fig. S16, ESI†) exhibits a shielding (blue) region connecting Ge7 and Ge11 atoms in the central diamond, which does not involve Cu1 and Cu2, supporting that  $\text{Cu}_2\text{Ge}_2$  is an overall antiaromatic section. Using  $\mathbf{B}_z^{\text{ind}}$ , the overall antiaromatic character in  $\text{Cu}_2\text{Ge}_2$  is denoted, resulting in a deshielding region comprising its four members, supporting the positive  $\text{NICS}_{\text{zz}}$  values depicted above.

Finally, we have performed a topological analysis of the electron density of the  $\{[\text{CuGe}_9\text{Mes}]_2\}^{4-}$  cluster.<sup>20</sup> The isosurface of the Laplacian (Fig. S17, ESI†) reveals a highly localized structure in the  $\text{Cu}_2\text{Ge}_2$  moiety, which agrees with the antiaromatic character of this fragment. The most delocalized regions correspond to the  $\pi$ -aromatic rings of the organic ligand. The multicenter indices<sup>21,22</sup> confirm these results, giving a large  $I_{\text{ring}}$  value (0.036) for the  $\pi$ -aromatic ring and a small value (0.004) for

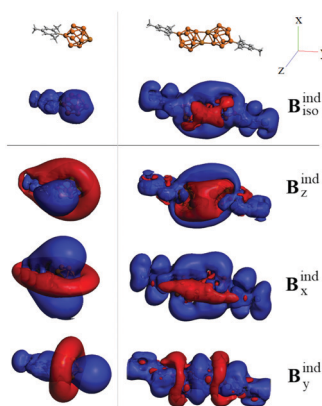


Fig. 5 Isosurface representation ( $\pm 2$  ppm) of the induced magnetic field, accounting for the isotropic and specific orientation of the field. Blue: shielding; red, deshielding.

$\text{Cu}_2\text{Ge}_2$ . The latter value and the bond-order alternation (BOA = 0.23) along the perimeter of the ring indicate that this moiety is antiaromatic. The topological analysis of the electron density (see the two ring critical points inside the  $\text{Cu}_2\text{Ge}_2$  moiety in Fig. S17, ESI<sup>†</sup>) shows that  $\text{Cu}_2\text{Ge}_2$  is composed of two ring structures (Cu–Ge–Cu). The latter exhibits positive  $I_{\text{ring}}$  values (0.04), indicating the 3c-2e nature of these interactions that was previously found by the AdNDP analysis. Conversely, neither the Laplacian of the electron density nor the multicenter indices attribute a large aromatic character to the  $\text{Ge}_9\text{Cu}$  cage, although the MCI value of the  $\text{Ge}_4\text{Cu}$  fragment (0.01) can be considered mildly aromatic.

In summary, the  $[\text{K}(2,2,2\text{-crypt})]_4[[\text{CuGe}_9\text{Mes}]_2](\text{DMF})_3$  species was structurally characterized, exposing the spontaneous formation of the dimeric  $\{[\text{CuGe}_9\text{Mes}]_2\}^{4-}$  cluster avoiding oxidative coupling. The parent  $[\text{CuGe}_9\text{Mes}]^{2-}$  monomer exhibits two aromatic motifs given by the organic mesityl-ligand and the deltahedral  $\text{CuGe}_9$  cage. Interestingly, the dimer formation stands on a central  $\sigma$ -antiaromatic  $\text{Cu}_2\text{Ge}_2$  diamond-like structure, involving two  $\text{Cu}_2\text{Ge}$  3c-2e  $\sigma$ -aromatic islands. Such features enable the characterization of the first example of an all-metal  $\sigma$ -antiaromatic species, as a stable structural motif bringing together two organic-Zintl aromatic sides.

This work was supported by the National Natural Science Foundation of China (No. 21971118 and 21722106) and the USA National Science Foundation (Grant CHE-1664379 to A. I. B.). A. M.-C. received funds from Fondecyt 1180683. E. M. acknowledges support from PGC2018-098212-B-C21 and EUR2019-103825 grants. The authors thank Prof. Slavi C. Sevov for valuable discussion and suggestions. The authors also thank the reviewers for comments on the discussion of Wade–Mingos rules.

## Conflicts of interest

There are no conflicts to declare.

## Notes and references

- (a) J. C. Santos, W. Tiznado, R. Contreras and P. Fuentealba, *J. Chem. Phys.*, 2004, **120**, 1670; (b) A. I. Boldyrev and L. S. Wang, *Chem. Rev.*, 2005, **105**, 3716; (c) M. Garcia-Borras, S. Osuna, J. M. Luis, M. Swart and M. Sola, *Chem. Soc. Rev.*, 2014, **43**, 5089; (d) J. M. Mercero, A. I. Boldyrev, G. Merino and J. M. Ugalde, *Chem. Soc. Rev.*, 2015, **44**, 6519; (e) C. Liu, I. A. Popov, Z. Chen, A. I. Boldyrev and Z. M. Sun, *Chem. – Eur. J.*, 2018, **24**, 14583.
- This data is based on our search results by web of science on November 21th, 2019. For more details see Fig. S15 (ESI<sup>†</sup>).
- (a) R. Breslow, *Chem. Eng. News*, 1965, **43**, 90; (b) R. Breslow, *Acc. Chem. Res.*, 1973, **6**, 393; (c) M. D. Peeks, M. Jirasek, T. D. W. Claridge and H. L. Anderson, *Angew. Chem., Int. Ed.*, 2019, **58**, 15717.
- 4 A. E. Kuznetsov, K. A. Birch, A. I. Boldyrev, X. Li, H. J. Zhai and L. S. Wang, *Science*, 2003, **300**, 622.
- 5 J. M. Mercero, M. Piris, J. M. Matxain, X. Lopez and J. M. Ugalde, *J. Am. Chem. Soc.*, 2009, **131**, 6949.
- 6 (a) A. N. Alexandrova and A. I. Boldyrev, *J. Phys. Chem. A*, 2003, **107**, 554; (b) D. Y. Zubarev and A. I. Boldyrev, *Phys. Chem. Chem. Phys.*, 2008, **10**, 5207.
- 7 I. A. Popov and A. I. Boldyrev in *The Chemical Bond: Chemical Bonding Across the Periodic Table*, ed. G. Frenking and S. Shaik, Wiley-VCH, 2014, vol. 14, p. 421.
- 8 E. Von Steuber, G. Elter, M. Noltemeyer, H. G. Schmidt and A. Meller, *Organometallics*, 2000, **19**, 5083.
- 9 (a) E. Maslowsky, *Coord. Chem. Rev.*, 2011, **255**, 2746; (b) S. Blanchard, L. Fensterbank, G. Gontard, E. Lacote, G. Maestri and M. Malacria, *Angew. Chem., Int. Ed.*, 2014, **53**, 1987; (c) Y. Wang, A. Monfredini, P. A. Deyris, F. Blanchard, E. Derat, G. Maestri and M. Malacria, *Chem. Sci.*, 2017, **8**, 7394; (d) C. Liu, N. V. Tkachenko, I. A. Popov, N. Fedik, X. Min, C. Q. Xu, J. Li, J. E. McGrady, A. I. Boldyrev and Z. M. Sun, *Angew. Chem., Int. Ed.*, 2019, **58**, 8367; (e) N. V. Tkachenko, X. W. Zhang, L. Qiao, C. C. Shu, D. Steglenko, A. Munoz-Castro, Z. M. Sun and A. I. Boldyrev, *Chem. – Eur. J.*, 2020, **26**, 2073.
- 10 (a) C. Liu, L. Li, I. A. Popov, R. J. Wilson, C. Xu, J. Li, A. I. Boldyrev and Z. M. Sun, *Chin. J. Chem.*, 2018, **36**, 1165; (b) L. Li, B. Ali, Z. Chen and Z. M. Sun, *Chin. J. Chem.*, 2018, **36**, 955; (c) X. Min, I. A. Popov, F. X. Pan, L. J. Li, E. Matito, Z. M. Sun, L. S. Wang and A. I. Boldyrev, *Angew. Chem., Int. Ed.*, 2016, **55**, 5531.
- 11 (a) E. Ruzin, A. Fuchs and S. Dehnen, *Chem. Commun.*, 2006, 4796; (b) S. Scharfe and T. F. Fässler, *Eur. J. Inorg. Chem.*, 2010, 1207; (c) Z. M. Sun, Y. F. Zhao, J. Li and L. S. Wang, *J. Cluster Sci.*, 2009, **20**, 601.
- 12 (a) C. Downie, Z. J. Tang and A. M. Guloy, *Angew. Chem., Int. Ed.*, 2000, **39**, 338; (b) T. F. Fässler and U. Schutz, *Inorg. Chem.*, 1999, **38**, 1866; (c) A. Ugrinov and S. C. Sevov, *J. Am. Chem. Soc.*, 2002, **124**, 10990; (d) A. Ugrinov and S. C. Sevov, *Inorg. Chem.*, 2003, **42**, 5789.
- 13 (a) C. Schenck, F. Henke, G. Santiso-Quinones, I. Krossing and A. Schnepf, *Dalton Trans.*, 2008, 4436; (b) F. Li and S. C. Sevov, *Inorg. Chem.*, 2015, **54**, 8121; (c) L. G. Perla, A. Muñoz-Castro and S. C. Sevov, *J. Am. Chem. Soc.*, 2017, **139**, 15176.
- 14 R. J. Wilson, L. Broeckaert, F. Spitzer, F. Weigend and S. Dehnen, *Angew. Chem., Int. Ed.*, 2016, **55**, 11775.
- 15 S. Scharfe, T. F. Fässler, S. Stegmaier, S. D. Hoffmann and K. Ruhland, *Chem. – Eur. J.*, 2008, **14**, 4479.
- 16 N. V. Tkachenko and A. I. Boldyrev, *Phys. Chem. Chem. Phys.*, 2019, **21**, 9590.
- 17 N. V. Tkachenko and A. I. Boldyrev, *Chem. Sci.*, 2019, **10**, 5761.
- 18 (a) K. Wade, *Chem. Commun.*, 1971, 210; (b) K. Wade, *Adv. Inorg. Chem. Radiochem.*, 1976, **16**, 1; (c) D. M. P. Mingos, *Nat. Phys. Sci.*, 1972, **236**, 99.
- 19 (a) F. Feixas, E. Matito, M. Duran, J. Poater and M. Sola, *Theor. Chem. Acc.*, 2010, **128**, 419; (b) F. Feixas, E. Matito, J. Poater and M. Sola, *Chem. Soc. Rev.*, 2015, **44**, 6434.
- 20 R. F. W. Bader, *Atoms in Molecules: A Quantum Theory*, Oxford University Press, Oxford, 1990.
- 21 M. Giambiagi, M. S. de Giambiagi, C. D. dos Santos Silva and A. P. de Figueredo, *Phys. Chem. Chem. Phys.*, 2000, **2**, 3381.
- 22 (a) P. Bultinck, R. Ponec and S. Van Damme, *J. Phys. Org. Chem.*, 2005, **18**, 706; (b) J. Ciosowski, E. Matito and M. Sola, *J. Phys. Chem. A*, 2007, **111**, 6521.